Journal of
Synchrotron Radiation

ISSN 0909-0495

Received 3 August 2007
Accepted 3 October 2007

Quantitative estimation of thermal contact conductance of a real front-end component at SPring-8 front-ends

Mutsumi Sano,[a]* Sunao Takahashi,[a] Tetsuro Mochizuki,[a] Atsuo Watanabe,[a] Masaki Oura[b] and Hideo Kitamura[a,b]

[a]JASRI, SPring-8, 1-1-1 Kouto, Sayo-cho, Sayo-gun, Hyogo 679-5198, Japan, and [b]RIKEN SPring-8 Center, 1-1-1 Kouto, Sayo-cho, Sayo-gun, Hyogo 679-5148, Japan. E-mail: musano@spring8.or.jp

The thermal contact conductance (TCC) of a real front-end component at SPring-8 has been quantitatively estimated by comparing the results of experiments with those of finite-element analyses. In this paper one of the methods of predicting the TCC of a real instrument is presented. A metal filter assembly, which is an indirect-cooling instrument, was selected for the estimation of the TCC. The temperature of the metal filter assembly for the maximum heat load of synchrotron radiation was calculated from the TCC that is expected under normal conditions. This study contributes towards the ongoing research program being conducted to investigate the real thermal limitation of all front-end high-heat-load components.

Keywords: front-end component; thermal contact conductance; metal filter assembly; electron beam; finite-element analysis.

1. Introduction

Some front-end components receive a high heat load from the intense photon beam of third-generation synchrotron radiation sources. In general, the temperature distribution for a direct-cooling component, such as an absorber (Mochizuki *et al.*, 1998) and front-end *XY* slits (Oura *et al.*, 1998), can be estimated rather precisely from the source parameters, configuration of the components, material properties *etc.* On the other hand, in the case of an indirect-cooling instrument, it is difficult to predict the maximum temperature because of the existence of a contact surface whose thermal contact conductance (TCC) is unknown.

In the past, considerable experimental work related to the estimation of the TCC has been reported; however, almost all of the data were obtained using a conventional test bench (Assoufid & Khounsary, 1996; Khounsary *et al.*, 1997; Asano *et al.*, 1993; Marion *et al.*, 2004). Other experiments using a similar method were carried out at temperatures close to that of liquid helium (Salerno *et al.*, 1984, 1993, 1994). Because such instrumentation typically comprised a hydraulic or pneumatic loading unit and small samples to ensure an ideal and uniform thermal contact, it was convenient to compare the experimental results with the theoretical ones. However, this instrumentation can only provide a first-order estimation of the TCC of a real system.

Hence, the aim of this study is to present an approximate value of the TCC for a general bolted clamping component manufactured using conventional machining and assembling technology. Although it is well known that the TCC is influenced by many factors, in the present study we focused on the surface roughness of the contact areas, fastening torque and interstitial materials. The TCCs were estimated by comparing the experiments with simulations using finite-element methods (FEMs). In the experiments the temperature drop between a heated part by the electron beam and a cooling part was measured near the interface. The simulations using FEMs were carried out by considering the TCC to be a parameter.

We chose a metal filter assembly (MFA) as a typical indirect-cooling component with a general bolted clamping method. The MFA, installed in the elliptical multipole wiggler beamline BL08W at SPring-8 (Maréchal *et al.*, 1998), is used to cut the low-energy part of the synchrotron radiation so that the heat load on the optical components is reduced. The maximum heat load on the MFA is estimated to be approximately 200 W mm^{-2} for normal incidence of the intense photon beam. The MFA consists of an absorbing filter made of aluminium and a cooling holder made of oxygen-free high-conductivity copper (OFHC), both of which are connected through a number of bolted joints. Therefore the thermal resistance of the MFA is determined on the basis of the heat transfer at the interface.

2. Experiment

2.1. Electron beam irradiation system

Fig. 1 shows the experimental apparatus. The experiments were carried out using an electron beam irradiation system composed of an electron gun, a beam stopper, a sample

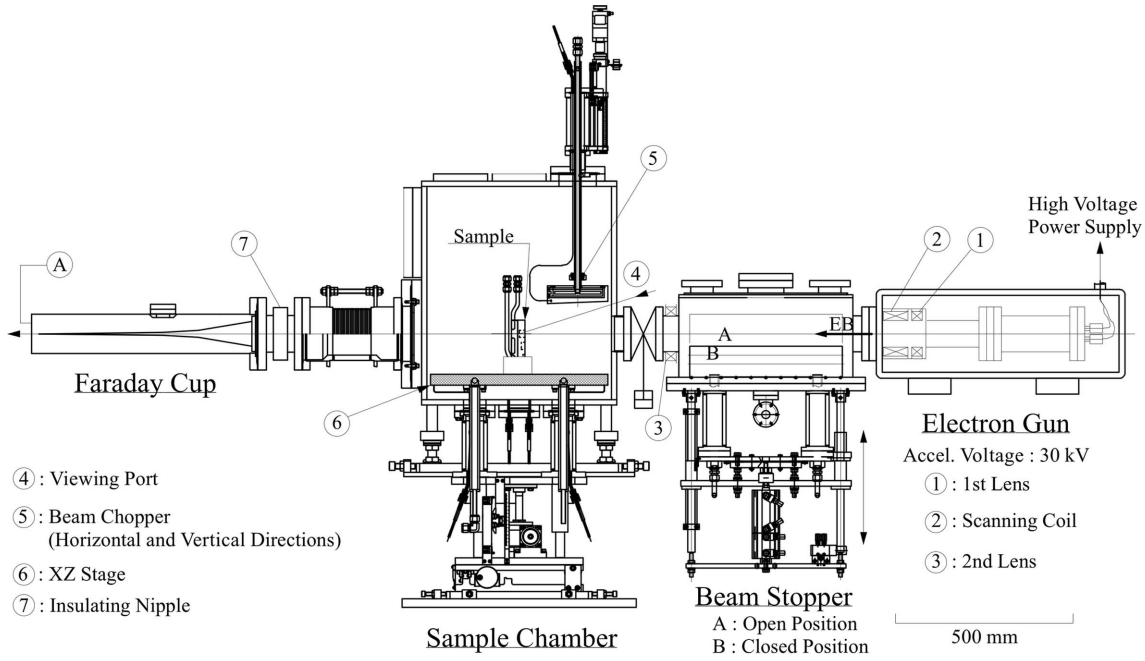

Figure 1
Schematic drawing of the electron beam irradiation system.

chamber and a Faraday cup. Electrons accelerated up to 30 keV are focused by the first magnetic lens. In order to obtain a uniform electron beam, scanning coils are installed along both the horizontal and vertical directions downstream of the first lens. The maximum scanning angles are $\pm 2.8^\circ$ for both directions, and the scanning frequencies for the horizontal and vertical directions are 100 Hz and 1 kHz, respectively. The beam stopper, which is capable of fully intercepting an electron beam, is driven by a pneumatic actuator. There is a second lens and a pneumatic gate valve downstream of the beam stopper. The pneumatic gate valve maintains a high vacuum in both the electron gun and the beam stopper chamber during the exchange of samples. The sample chamber is composed of an *XZ* stage, beam choppers, viewing ports and thermocouples. The *XZ* stage is used to fix the samples, and the sample position can be adjusted by driving the *XZ* stage. The maximum driving distance in the vertical direction is 100 mm, while in the horizontal direction it is approximately ± 5 mm relative to the original position. A typical sample position is approximately 1 m from the exit of the electron gun. The beam choppers, which are used to determine the beam profiles, are installed along the horizontal and vertical directions. They can be driven by stepping motors to obtain their precise positions. The thermocouples, which are provided by vacuum port feedthroughs, monitor the sample temperatures. The Faraday cup, which is used to monitor the electron beam current, is connected to the sample chamber through an insulating nipple. The beam stopper, beam choppers and Faraday cup are made of OFHC and have inclined surfaces for the irradiated parts in order to reduce the high heat flux density of the electron beam. Both the beam stopper chamber and the sample chamber are independently pumped by 1500 L s^{-1} cryopumps. The base pressures of the beam stopper chamber and the sample chamber are approximately 3×10^{-6} Pa and 1×10^{-5} Pa, respectively.

2.2. Measurement of the temperature drop

A schematic drawing of the MFA is shown in Fig. 2. The aluminium absorbing filter and the OHFC cooling holder are connected by 28 bolts of size M5. There are three kinds of filtering parts with thicknesses of 5 mm, 10 mm and 15 mm. The part with a thickness of 5 mm is normally used. A copper pipe, whose internal diameter is 8 mm, is brazed to the cooling holder and acts as the cooling channel. Three sets of samples with different roughnesses of the contact surface were prepared by the same design and manufacturing process as that used for the real MFA. Fig. 3 shows the experimental set-up inside the sample chamber. A vertically scanning electron beam with a frequency of 1 kHz was produced as the incident beam. The scanning was performed in a triangular wave. The beam profile in the horizontal direction was measured by the beam chopper and the Faraday cup, as shown in Fig. 4. A tantalum slit, whose aperture size is 12 mm (H) $\times$ 30 mm (V), is installed on the upstream side of the filter in order to restrict the absorbing area. The real absorbed power is calculated from the flow rate and the temperature difference between the inlet and outlet of the cooling water. We measured the temperature drop between the absorbing filter and the cooling holder using the thermocouples, which were embedded in both of them at a distance of 2 mm from the interface. The thermocouples used for the cooling water were of the T-type, while those used for the samples were of the K-type. The diameters of the sheaths for the T-type and the K-type are 1.6 mm and 1.0 mm, respectively.

The experimental parameters were as follows.

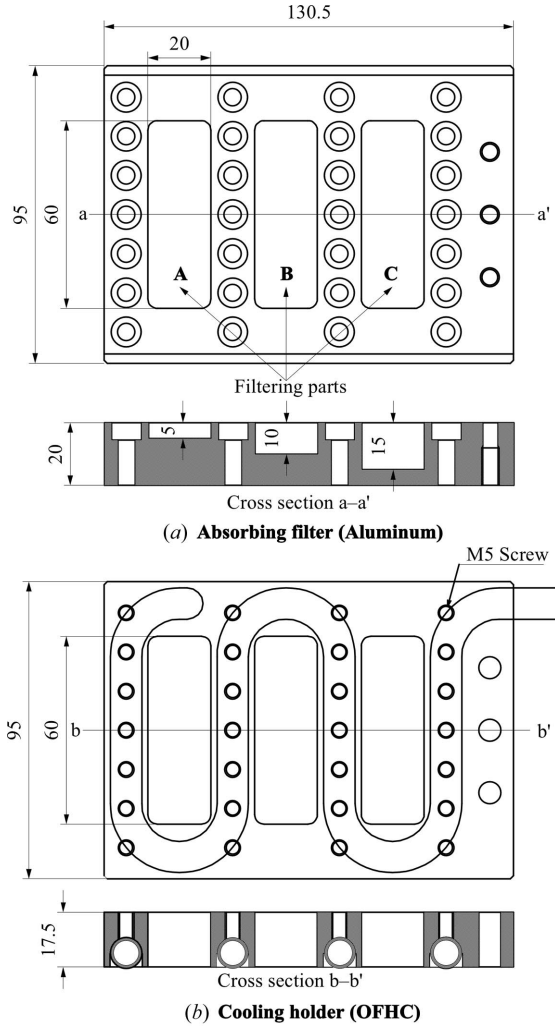

Figure 2
Schematic drawing of the MFA. Cross sections are shown for both the absorbing filter and the cooling holder. The thicknesses of the filtering parts *A*, *B* and *C* are 15 mm, 10 mm and 5 mm, respectively.

(i) Surface roughness (Ra): 0.2 µm, 1.6 µm and 12.5 µm.

(ii) Interstitial material: 50 µm-thick gold foil, 20 µm-thick gold foil, 50 µm-thick silver foil, and no interstitial material.

(iii) Fastening torque: 1 N m, 3 N m and 6 N m.

(iv) Absorbed power: 440 W.

(v) Flow rate of the cooling water: 4 L min^{-1}.

An indium sheet, which is one of the popular interstitial materials, was not selected because its melting point of 429.6 K is too low for our case.

Averaged contact pressures of the MFA for the above fastening torques were estimated to be approximately 0.8 MPa, 2 MPa and 4 MPa, respectively, by using a Fujifilm Prescale Pressuregraphe FPD-9210. Fig. 5 shows an example of a pressure distribution measured using the Prescale when the fastening torque is 3 N m for Ra = 1.6 µm. The pressure range of the Prescale is from 0.5 MPa to 2.5 MPa.

Because of the measurement method adopted for determining the absorbed power, it is necessary to know the relative temperature difference between both the T-type thermocouples as precisely as possible. We have confirmed,

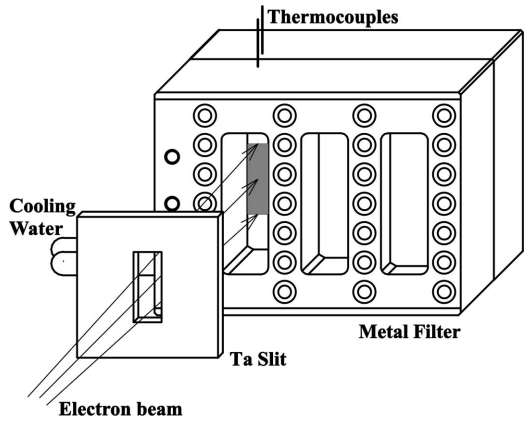

Figure 3
Experimental set-up inside the sample chamber.

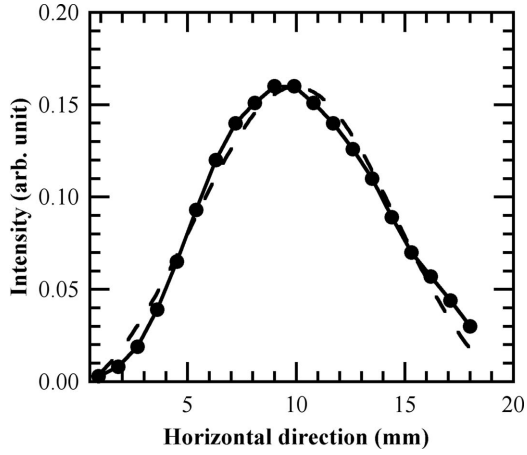

Figure 4
Electron beam profile in the horizontal direction. The closed circles with line are fitted by a Gaussian function as shown by the dashed line.

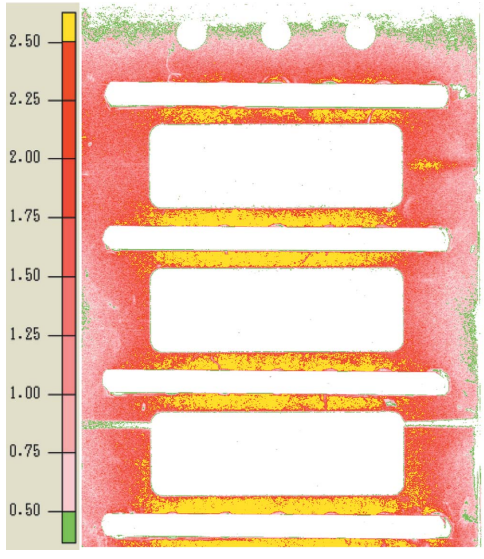

Figure 5
Pressure distribution for Ra = 1.6 µm measured using the Prescale. The fastening torque is 3 N m.

Table 1
Temperature drops between the aluminium filter and the OFHC holder for each set-up of the MFA.

The upper row shows the minimum and the maximum temperature drops. The lower row shows their averaged values and the standard deviations.

	Temperature drop (K)			
	Interstitial material			
Ra, torque	Au (50 µm)	Au (20 µm)	Ag (50 µm)	None
0.2 µm, 1 N m	4.8–8.6	–	–	7.2–11.4
	6.4 ± 1.2	–	–	9.1 ± 1.3
0.2 µm, 3 N m	3.5–4.8	1.8–2.9	2.5–2.8	4.5–6.2
	4.5 ± 0.4	2.5 ± 0.4	2.6 ± 0.1	5.5 ± 0.5
0.2 µm, 6 N m	2.1–3.4	–	–	3.2–4.2
	3.1 ± 0.4	–	–	3.9 ± 0.4
1.6 µm, 3 N m	2.6–4.0	1.9–3.4	2.5–5.0	1.8–2.6
	3.1 ± 0.5	2.3 ± 0.4	2.9 ± 0.8	2.1 ± 0.3
12.5 µm, 1 N m	8.4–32.4	–	–	4.2–27.9
	17.7 ± 7.7	–	–	12.8 ± 9.0
12.5 µm, 3 N m	2.9–11.9	–	–	2.7–7.8
	7.2 ± 2.9	–	–	4.9 ± 1.8
12.5 µm, 6 N m	2.4–5.0	–	–	1.8–6.5
	3.9 ± 0.8	–	–	3.5 ± 1.4

from calibrations using a constant temperature bath, that the relative difference between these thermocouples was within approximately 0.01 K. The relative temperature difference between the K-type thermocouples was within approximately 0.1 K. This value was obtained from calibrations by measuring the temperature of a copper block heated by the electron beam using these K-type thermocouples. The temperatures of the sample and cooling water were recorded using a Yokogawa DR 230 Hybrid Recorder and a Keithley 2182 Nanovoltmeter, respectively. They were measured after stabilization. The measurements were repeated six to ten times for each set-up. The MFA was reassembled for every measurement. The diminishing surface roughness, owing to repeated tightening of the bolts, is little affected by the number of repetitions as no systematic change in the measured values was found as the number of repetitions increased. Table 1 shows the mean value for 1 min of temperature drops between the absorbing filter and the cooling holder for each set-up; the sampling time was 2 s. The standard deviations of each measured data set are within approximately 0.1 K. The upper row shows the minimum and the maximum temperature drops, while the lower row shows their averaged values and the standard deviations. The temperature drops for the 20 µm-thick gold foil and the 50 µm-thick silver foil were measured only for Ra = 0.2 µm and 1.6 µm when the fastening torque was 3 N m.

3. Finite-element analyses

3.1. Boundary conditions

We conducted thermal analyses using the finite-element program *ANSYS* (http://www.ansys.com). As shown in Fig. 6, we constructed a FEM model that resembled the real MFA as closely as possible. A surface-to-surface contact element, by which the TCC could be defined directly, was placed on the interface.

The thermal analyses were carried out under the following boundary conditions.

(i) The absorbed power was 440 W. The beam profile in the horizontal direction was fitted by a Gaussian distribution, as shown in Fig. 4. As a result, the power distribution was uniform in the vertical direction because of the constant scanning speed of the beam in a triangular pattern and the Gaussian distribution in the horizontal direction. The heat flux was set on the surface area of each element.

(ii) The irradiated area was set at 12 mm × 30 mm, corresponding to the aperture size of the tantalum slit.

(iii) The bulk temperature of the water was 306 K.

(iv) The heat transfer coefficient (h) of the cooling channels was 6900 W m^{-2} K^{-1} with a flow rate of 4 L min^{-1} and an internal diameter of 8 mm. The heat transfer coefficient was obtained from

$$h = \frac{\mathrm{Nu}\,\lambda}{d} = \frac{0.023(\mathrm{Re})^{0.8}(\mathrm{Pr})^{0.4}\lambda}{d}, \qquad (1)$$

where Nu is the Nusselt number, λ (W m^{-1} K^{-1}) is the thermal conductivity of water, d (m) is the internal diameter of the cooling channel, Re is the Reynolds number and Pr is the Prandtl number. The Dittus–Bolter equation shown in (1) was used for the Nusselt number.

(v) The parameter of TCC was varied within the range 2000 to 110000 W m^{-2} K^{-1}.

3.2. Estimation of TCC

Fig. 7 shows an example of an analysis result for a TCC of 10000 W m^{-2} K^{-1}. The temperature drop between the absorbing filter and the cooling holder for each TCC was calculated from the nodal solutions corresponding to the real thermocouple locations. Fig. 8 shows the relationship between

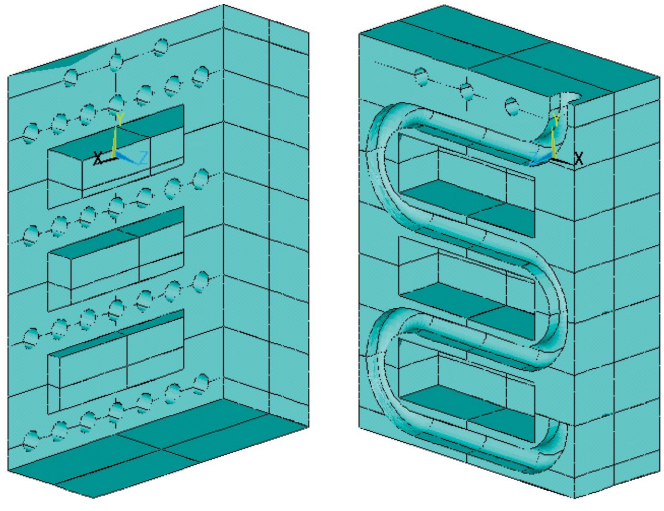

(*a*) (*b*)

Figure 6
FEM model of the MFA. (*a*) Absorbing filter side. (*b*) Cooling holder side.

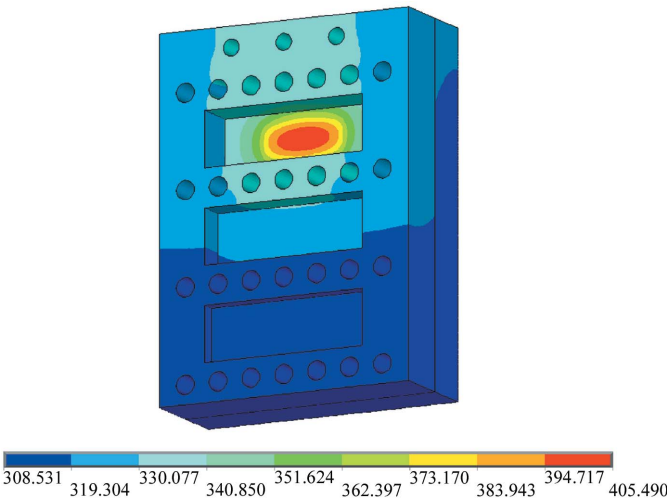

Figure 7
The temperature distribution of the MFA heated by the electron beam calculated from the nodal solution in the case of an absorbed power of 440 W and TCC of 10000 W m^{-2} K^{-1}.

the various TCCs and the temperature drop. Accordingly, actual TCCs could be assumed from each observed temperature drop using Fig. 8. Figs. 9 and 10 show the TCCs for each set-up of the MFA, which are estimated by applying the experimental results to Fig. 8. The symbols and the error bars indicate the averaged values and the standard deviations, respectively. The dependence of the TCC on the fastening torque is shown in Figs. 9(*a*) and 9(*b*) for the set-up with Ra = 0.2 µm and 12.5 µm. The MFA was set up for Ra = 0.2 µm and 12.5 µm, and for each set-up observations were made for the case where the 50 µm-thick gold foil was used and for the case without an interstitial material. It is apparent that for all set-ups of the MFA the TCC increases with the fastening torque owing to an increase in the actual contact area. It is also observed that the standard deviations in the case of Ra = 12.5 µm are larger than those for Ra = 0.2 µm. This result

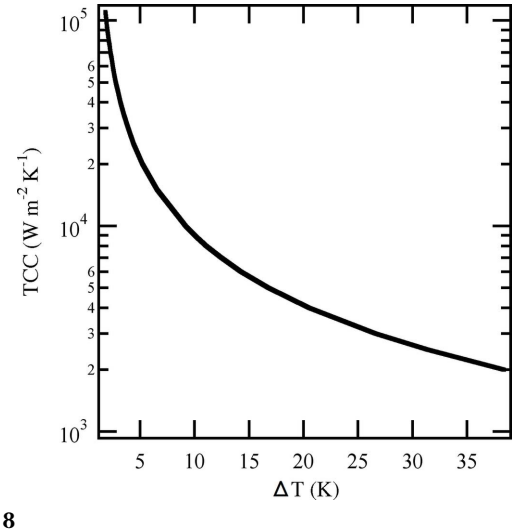

Figure 8
Relationship between the TCC and the temperature difference calculated from the nodal solutions at real thermocouple locations.

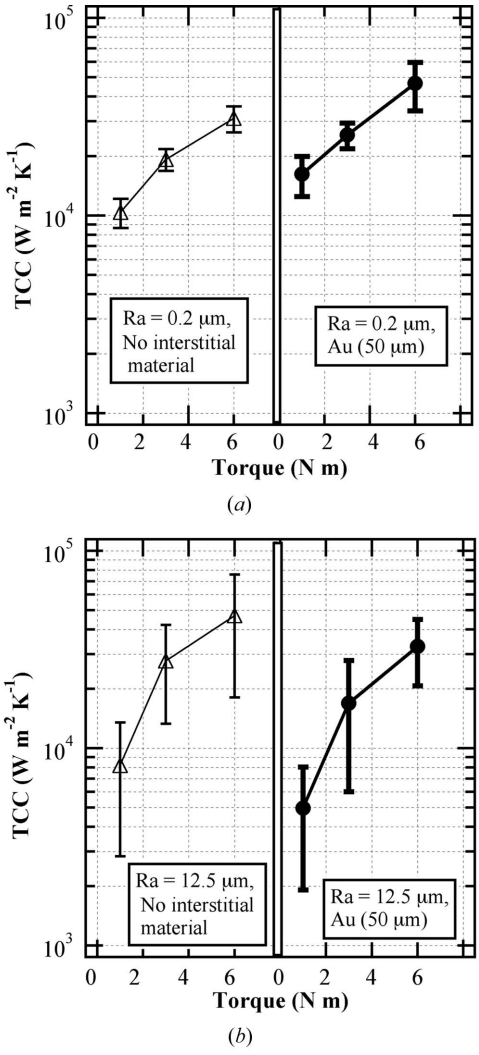

Figure 9
The fastening torque dependence of the TCC for Ra = 0.2 µm (*a*) and 12.5 µm (*b*). For each set-up the 50 µm-thick gold foil and no interstitial material was used. The symbols and the error bars indicate the averaged values and the standard deviations, respectively.

indicates that the contact condition between the rougher surfaces could change easily. When Ra = 0.2 µm, the TCCs for the 50 µm-thick gold foil are larger than those for no interstitial material for all fastening torques. On the other hand, it is noteworthy that, in the case of Ra = 12.5 µm and for a given fastening torque, the TCCs obtained by using the 50 µm-thick gold foil are smaller than those obtained in the absence of an interstitial material. Although the reason for the opposite tendencies exhibited for Ra = 0.2 µm and 12.5 µm irrespective of an interstitial material being used is unclear, some other factor that we could not control, such as the waviness of the contact surfaces, might have influenced these results.

Fig. 10 shows the TCCs for each interstitial material and surface roughness when the fastening torque is fixed at 3 N m. The appropriate fastening torque is 3 N m for a MFA clamped with M5-sized bolts. It is apparent that all the averaged TCC values exceed 10000 W m^{-2} K^{-1}. The largest TCCs for no interstitial material and the 50 µm-thick gold foil are observed when Ra = 1.6 µm. When both the 20 µm-thick gold foil and

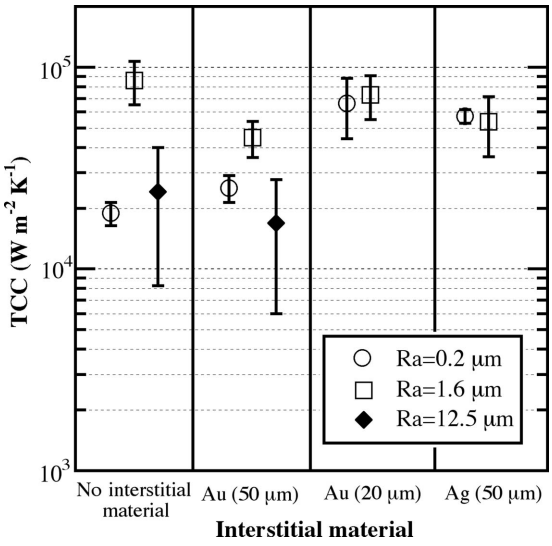

Figure 10
TCCs for each interstitial material and surface roughness when the fastening torque is 3 N m. The symbols and the error bars indicate the averaged values and the standard deviations, respectively.

50 μm-thick silver foil are used, the TCCs for Ra = 0.2 μm and 1.6 μm are close to each other. Besides, when the interstitial materials are used, it appears that the spread of the TCCs is fairly small except for the case for Ra = 12.5 μm. In other words, the interstitial material could minimize the impact of the individual differences between the contact surfaces. When comparing the case of the 50 μm-thick gold foil with that of the 20 μm-thick gold foil, it is found that the TCC in the latter case is larger than in the former case. This probably indicates that a thinner interstitial material improves the contact condition for a given material.

3.3. Evaluation for the real MFA

When the fastening torque is appropriate, *i.e.* 3 N m, we could expect from the above results that the average TCC values could exceed 10000 W m^{-2} K^{-1}. This result was applied to the thermal analysis of the maximum heat load of the synchrotron radiation of BL08W. The source parameters were as follows: beam current = 100 mA, gap = 25.5 mm, K_x = 0, K_y = 11.3, and total power = 18.3 kW. The MFA is at a distance of 28.71 m from the source. As shown in Fig. 11, the power density distributions were calculated for both the horizontal and the vertical directions at various distances of the MFA using the program code *SPECTRA* (Tanaka & Kitamura, 2001). The part of the MFA with a thickness of 5 mm, which is normally used, was selected as the absorbing part. The absorbing region could not be restricted to only the surface of the MFA, as in the electron beam case, because synchrotron radiation includes the hard X-ray region. The boundary conditions for the absorbed power were decided by considering both the energy spectrum at the centre of each element and the absorption coefficient of aluminium. The boundary conditions were given as the volumetric heat generation of each element. The total power absorbed by the MFA was 2.15 kW. The series of absorption calculations were taken from MacGillavry & Rieck (1962). With the heat transfer coefficient (h) of the cooling channels assumed to be 13000 W m^{-2} K^{-1}, with a flow rate of 9 L min^{-1}, a water temperature of 306 K and a TCC of 10000 W m^{-2} K^{-1}, the maximum temperature was estimated to be 763 K from FEM calculations. Fig. 12 shows the temperature distribution. Because the melting point of aluminium is 933 K, the MFA is operational. As shown in Fig. 10, when Ra = 12.5 μm using the 50 μm-thick gold foil, the TCC could become about 6000 W m^{-2} K^{-1} from the standard deviation. Even if the TCC is 6000 W m^{-2} K^{-1}, the maximum temperature of the MFA is calculated to be 797 K which is below the melting point. We validated the FEM results by confirming that the MFA has never melted, since there is no appropriate method of measuring the maximum temperature of the MFA directly.

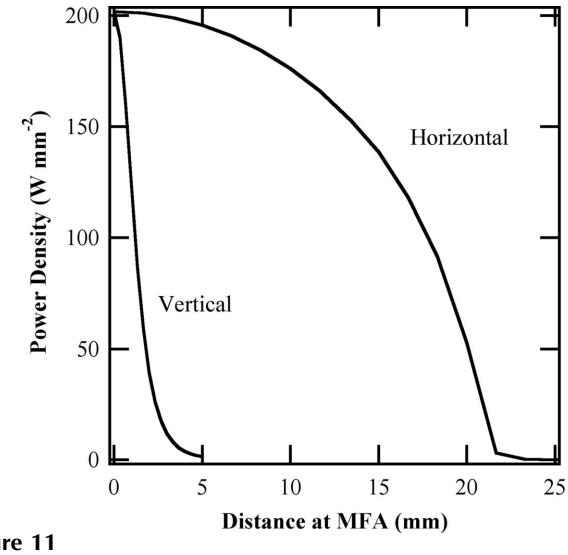

Figure 11
BL08W at SPring-8 power density distributions along the axis at various MFA distances. Source parameters: beam current = 100 mA, gap = 25.5 mm, K_x = 0, K_y = 11.3, total power = 18.3 kW.

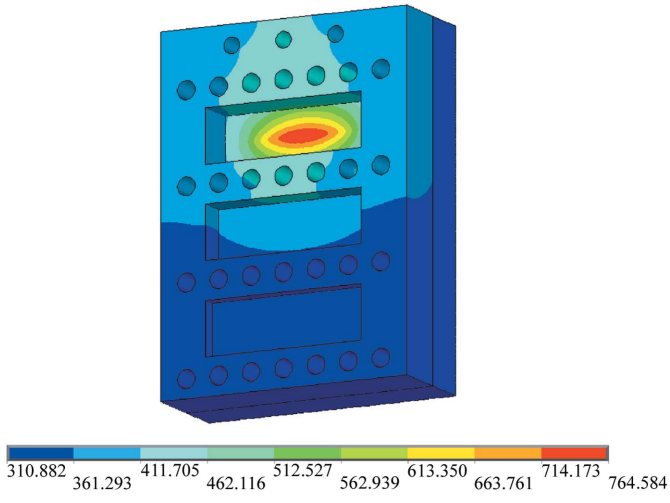

Figure 12
Temperature distribution of the MFA calculated from the nodal solution for the maximum heat load of the synchrotron radiation in the case of a TCC of 10000 W m^{-2} K^{-1}.

However, we could expect the MFA to be operated under safe conditions from the above results.

4. Conclusion

The TCC of a MFA, one of the indirect-cooling components of SPring-8 front-ends, has been examined by comparing the experimental results using an electron beam irradiation system with those of finite-element analysis under various contact conditions. As a result, regardless of the existence and type of the interstitial material, we confirmed that the actual value of the TCC for a general bolted clamping component such as the MFA could be assumed to be at least greater than $\sim 10000\ \mathrm{W\ m^{-2}\ K^{-1}}$, provided that the contact areas were finely finished and tightly fastened with the adequate recommended torque for the given bolt size.

References

Asano, M., Ogata, J. & Yosinaga, Y. (1993). *Proc. SPIE*, **1739**, 652–656.

Assoufid, L. & Khounsary, A. M. (1996). *Rev. Sci. Instrum.* **67**, 3354.

Khounsary, A. M., Chjnowski, D., Assoufid, L. & Worek, W. M. (1997). *Proc. SPIE*, **3151**, 45–51.

MacGillavry, C. H. & Rieck, G. D. (1962). *International Tables for X-ray Crystallography*, Volume III, *Physical and Chemical Tables*, pp. 157–200. Birmingham: Kynoch Press.

Maréchal, X.-M., Hara, T., Tanabe, T., Tanaka, T. & Kitamura, H. (1998). *J. Synchrotron Rad.* **5**, 431–433.

Marion, Ph., Zhang, L., Vallet, L. & Lesourd, M. (2004). *Third International Workshop on Mechanical Engineering Design of Synchrotron Radiation Equipment and Instrumentation (MEDSI2004)*, 24–27 May 2004, Grenoble, France. MEDSI-Proc-04–53.

Mochizuki, T., Sakurai, Y., Shu, D., Kuzay, T. M. & Kitamura, H. (1998). *J. Synchrotron Rad.* **5**, 1199–1201.

Oura, M., Sakurai, Y. & Kitamura, H. (1998). *J. Synchrotron Rad.* **5**, 606–608.

Salerno, L. J., Kittel, P. & Spivak, A. L. (1984). *AIAA J.* **22**, 1810–1816.

Salerno, L. J., Kittel, P. & Spivak, A. L. (1993). *Cryogenics*, **33**, 1104–1109.

Salerno, L. J., Kittel, P. & Spivak, A. L. (1994). *Cryogenics*, **34**, 649–654.

Tanaka, T. & Kitamura, H. (2001). *J. Synchrotron Rad.* **8**, 1221–1228.